

Supplementary Information

Synthesis and Characterization of Metal-Rich Phosphonium Polyelectrolytes and Their Use as Precursors to Nanomaterials

*Amir Rabiee Kenaree and Joe B. Gilroy**

Department of Chemistry and the Centre for Advanced Materials and Biomaterials Research
(CAMBR), The University of Western Ontario, 1151 Richmond St. N., London, Ontario,
Canada, N6A 5B7. Tel: +1-519-661-2111 ext. 81561; E-mail: joe.gilroy@uwo.ca.

Table of Contents

NMR spectra.....	S2
GPC data.....	S12
UV-vis absorption spectra.....	S13
Cyclic voltammograms.....	S15
Differential scanning calorimetry thermograms.....	S16
Element maps.....	S17
Scanning electron microscopy and energy-dispersive X-ray spectroscopy results.....	S20
Powder X-ray diffractograms.....	S24
References.....	S28

NMR spectra

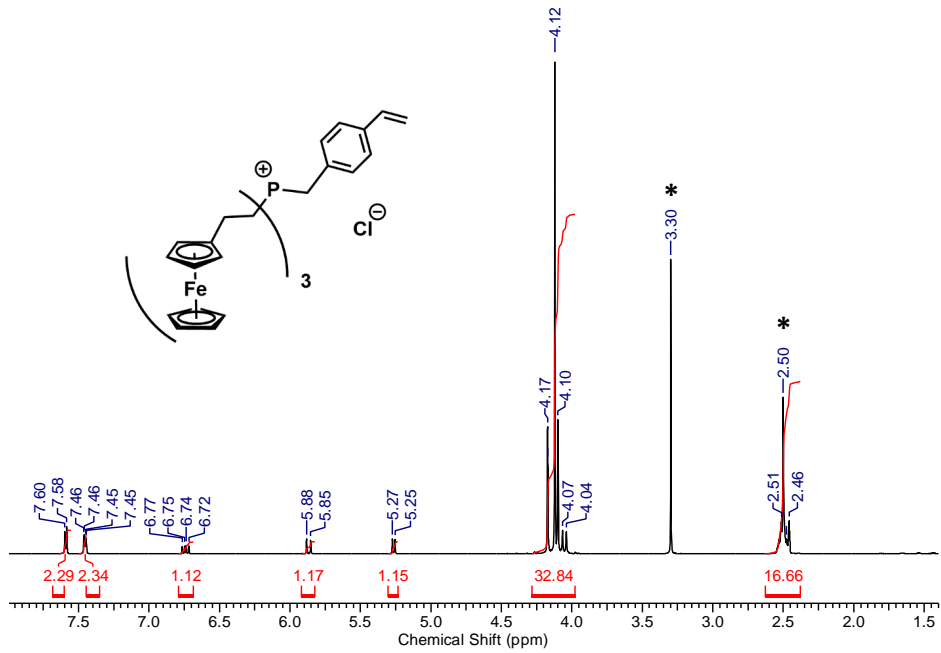


Fig. S1 ^1H NMR spectrum of **6a** in $\text{DMSO}-d_6$. The asterisks denote residual solvent signals.

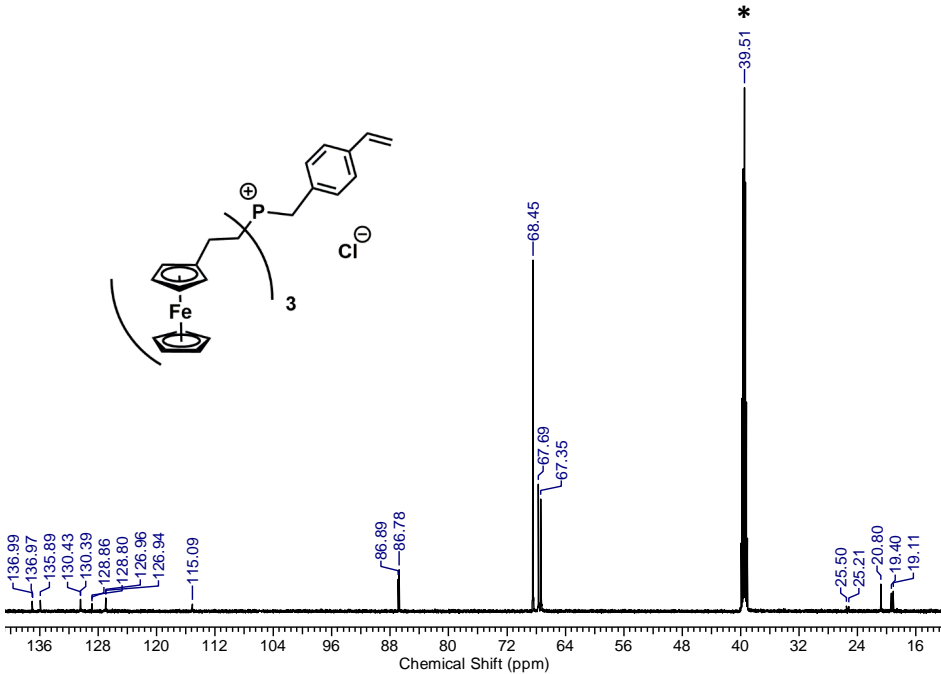


Fig. S2 $^{13}\text{C}\{^1\text{H}\}$ MR spectrum of **6a** in $\text{DMSO}-d_6$. The asterisk denotes the solvent signal.

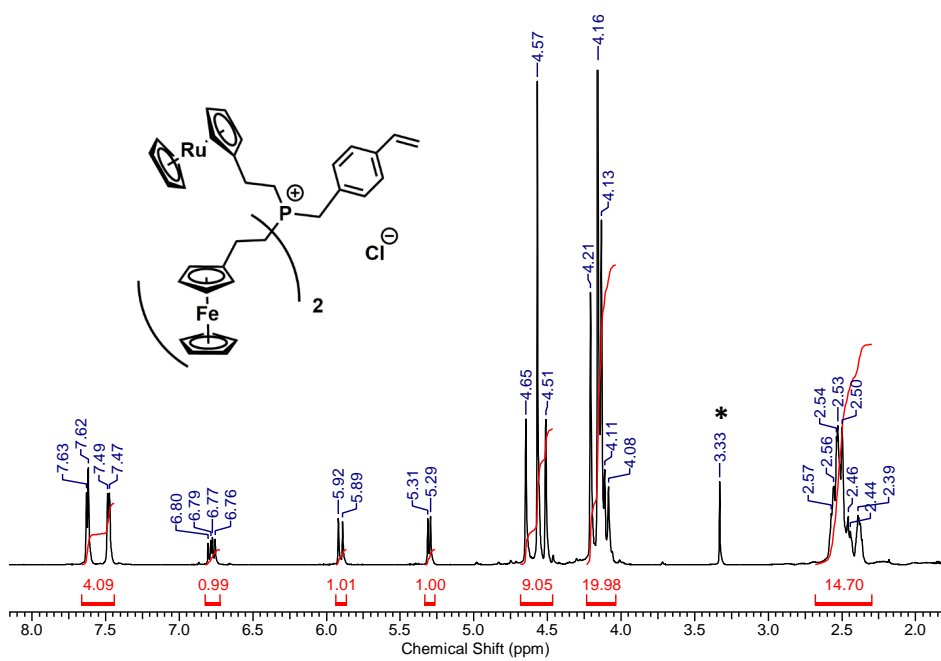


Fig. S3 ^1H NMR spectrum of **6b** in $\text{DMSO}-d_6$. The asterisks denote residual solvent signal.

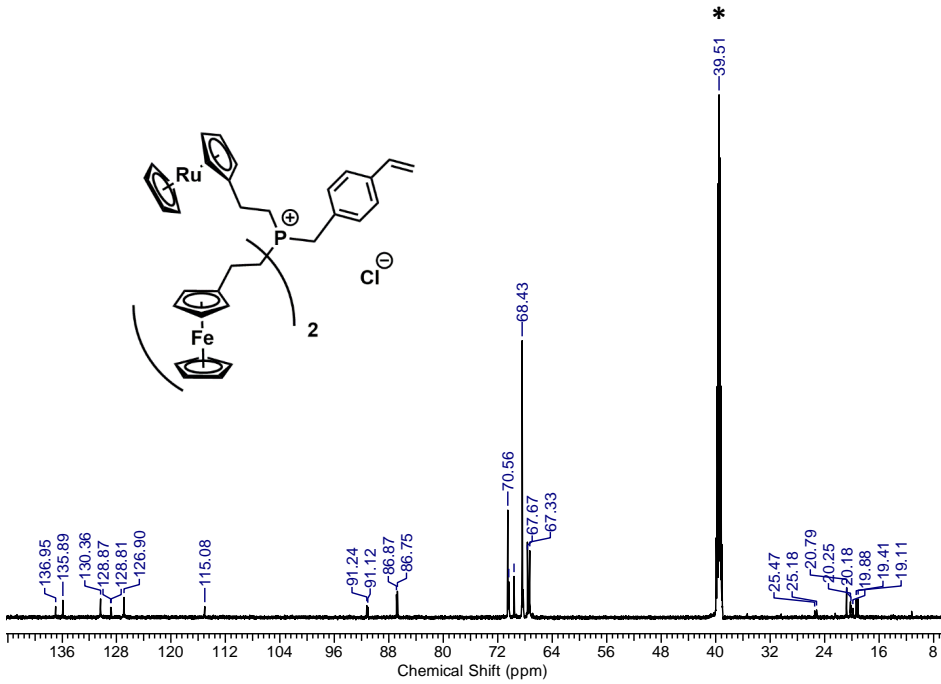


Fig. S4 $^{13}\text{C}\{^1\text{H}\}$ NMR spectrum of **6b** in $\text{DMSO}-d_6$. The asterisk denotes the solvent signal.

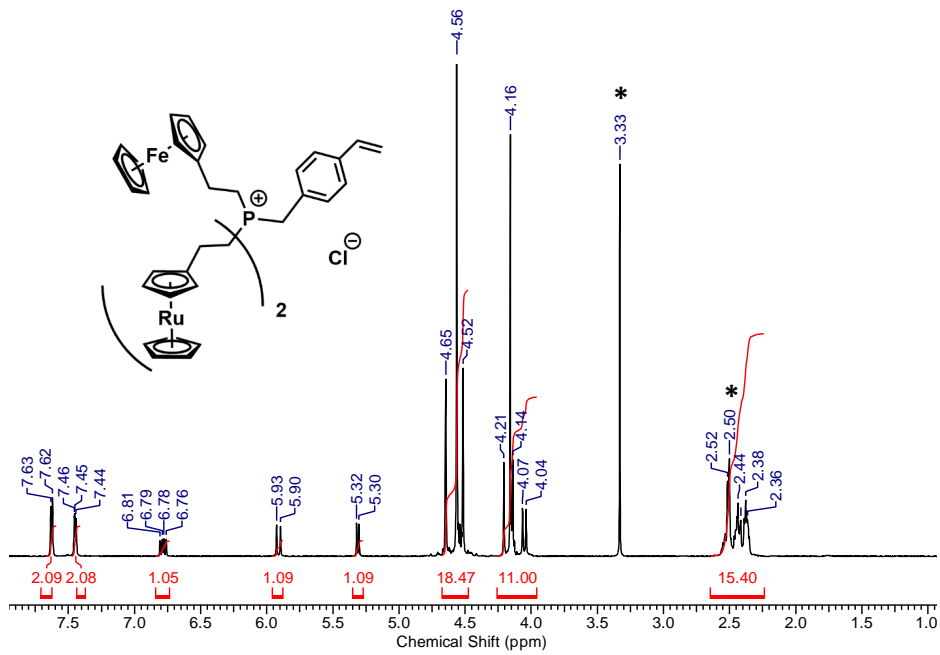


Fig. S5 ^1H NMR spectrum of **6c** in $\text{DMSO}-d_6$. The asterisks denote residual solvent signals.

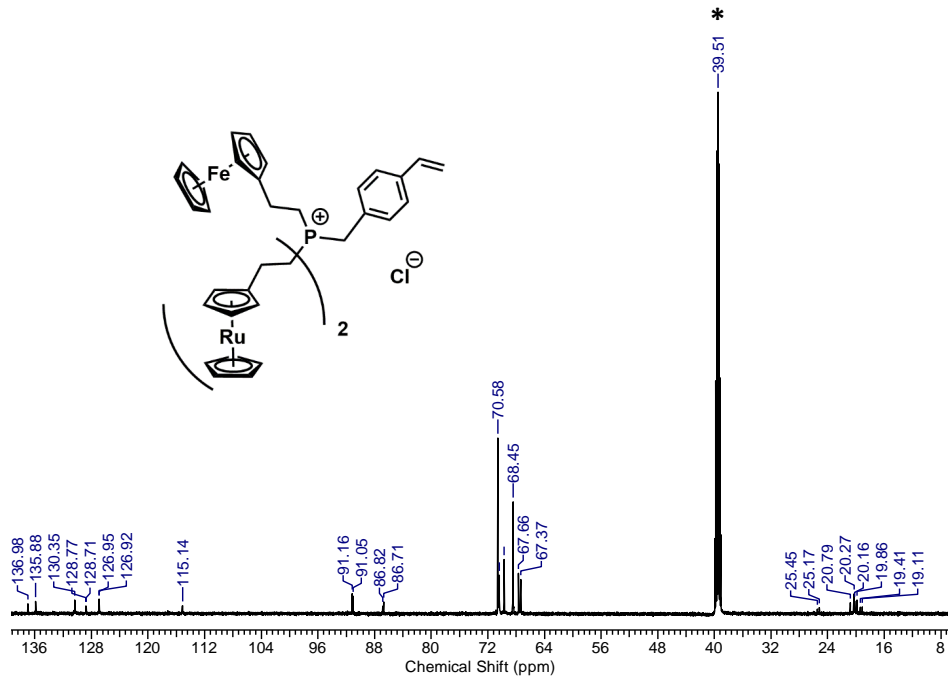


Fig. S6 $^{13}\text{C}\{^1\text{H}\}$ NMR spectrum of **6c** in $\text{DMSO}-d_6$. The asterisk denotes the solvent signal.

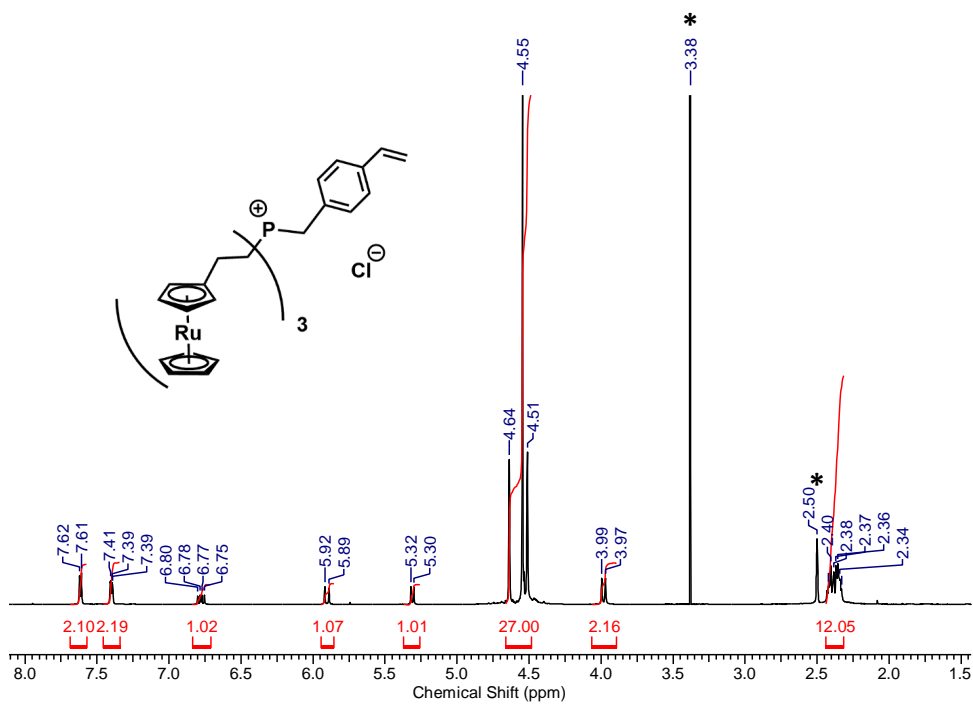


Fig. S7 ^1H NMR spectra of **6d** in $\text{DMSO}-d_6$. The asterisks denote residual solvent signals.

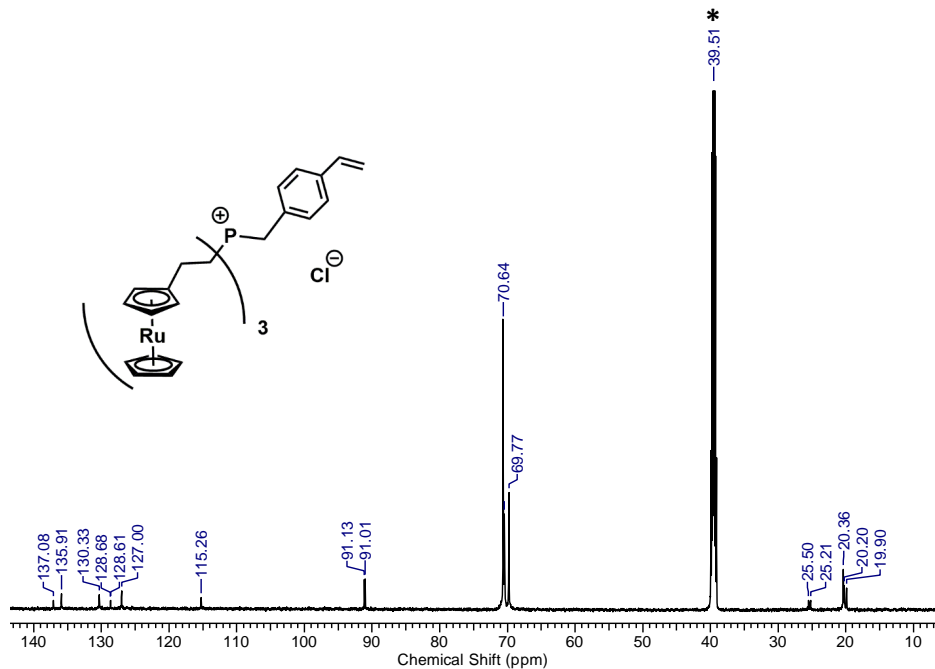


Fig. S8 $^{13}\text{C}\{^1\text{H}\}$ NMR spectrum of **6d** in $\text{DMSO}-d_6$. The asterisk denotes the solvent signal.

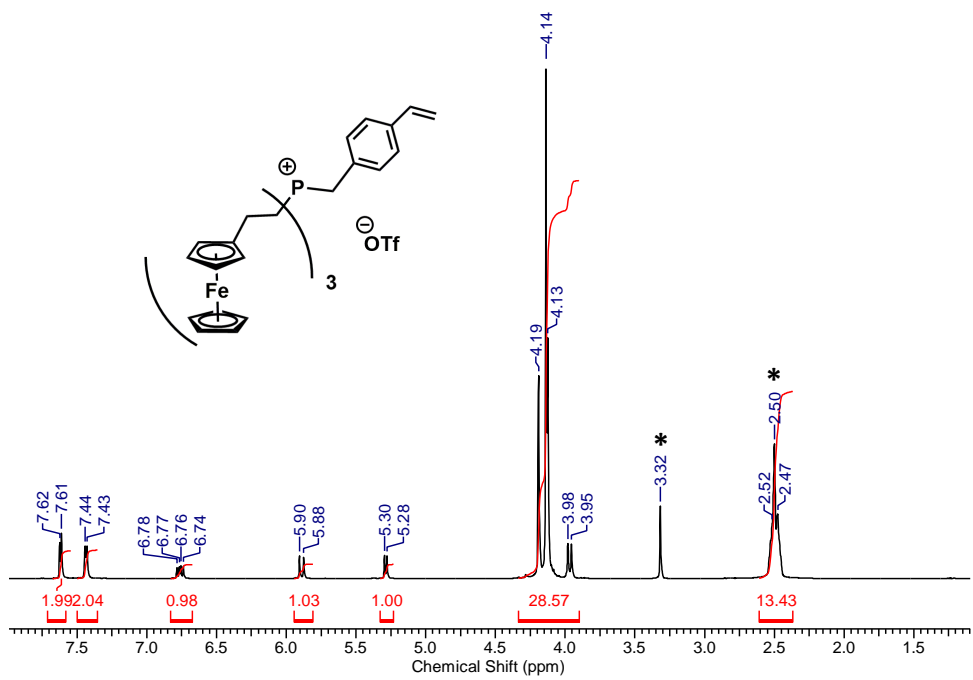


Fig. S9 ^1H NMR spectrum of **7a** in $\text{DMSO}-d_6$. The asterisks denote the solvent signals.

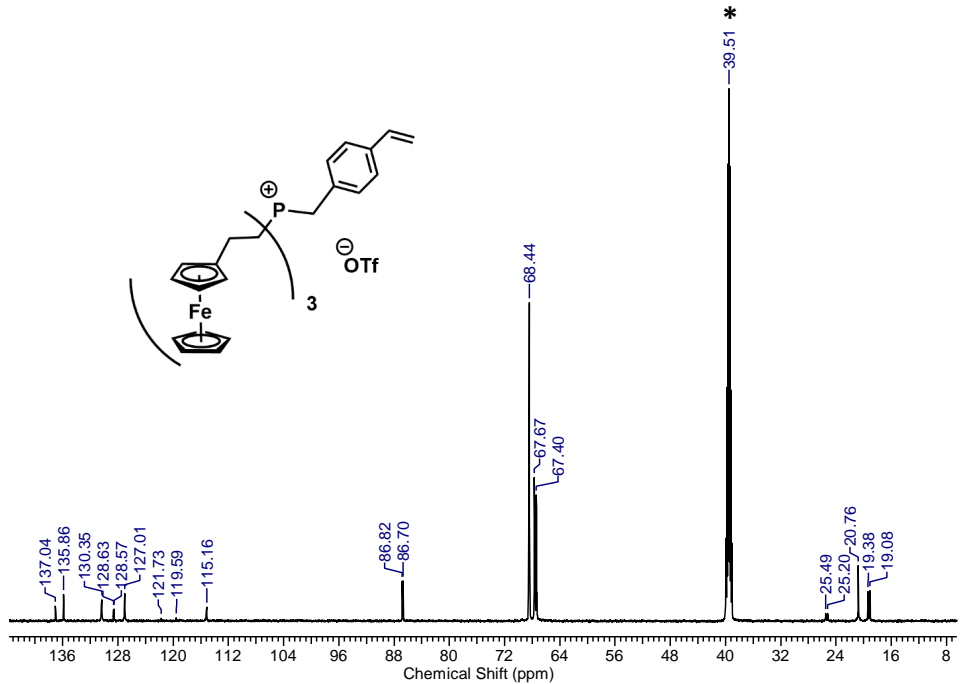


Fig. S10 $^{13}\text{C}\{^1\text{H}\}$ NMR spectrum of **7a** in $\text{DMSO}-d_6$. The asterisk denotes the solvent signal.

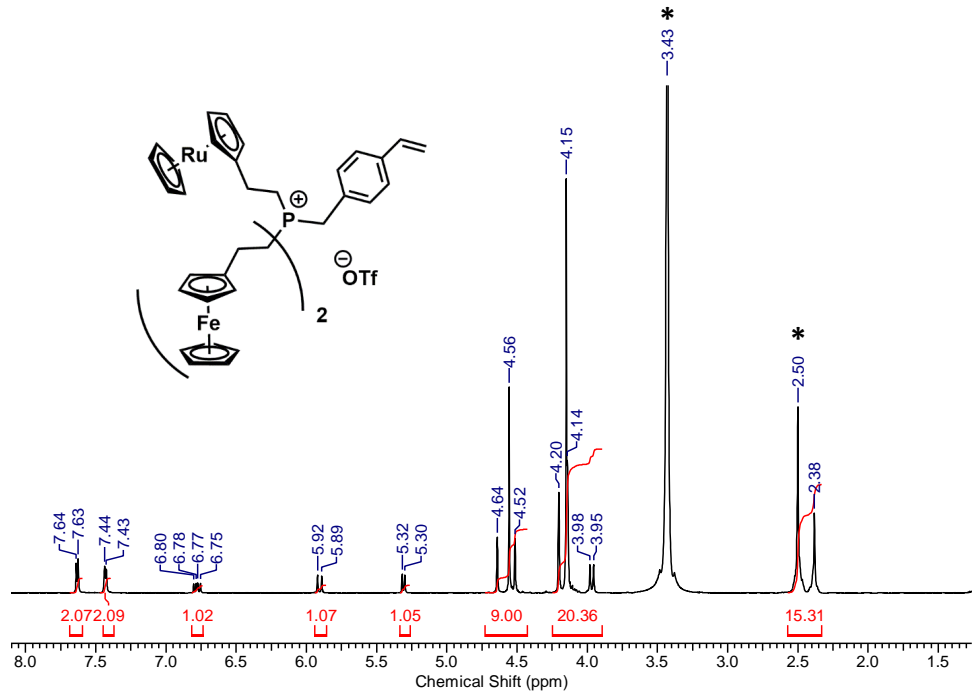


Fig. S11 ^1H NMR spectrum of **7b** in $\text{DMSO}-d_6$. The asterisks denote the solvent signals.

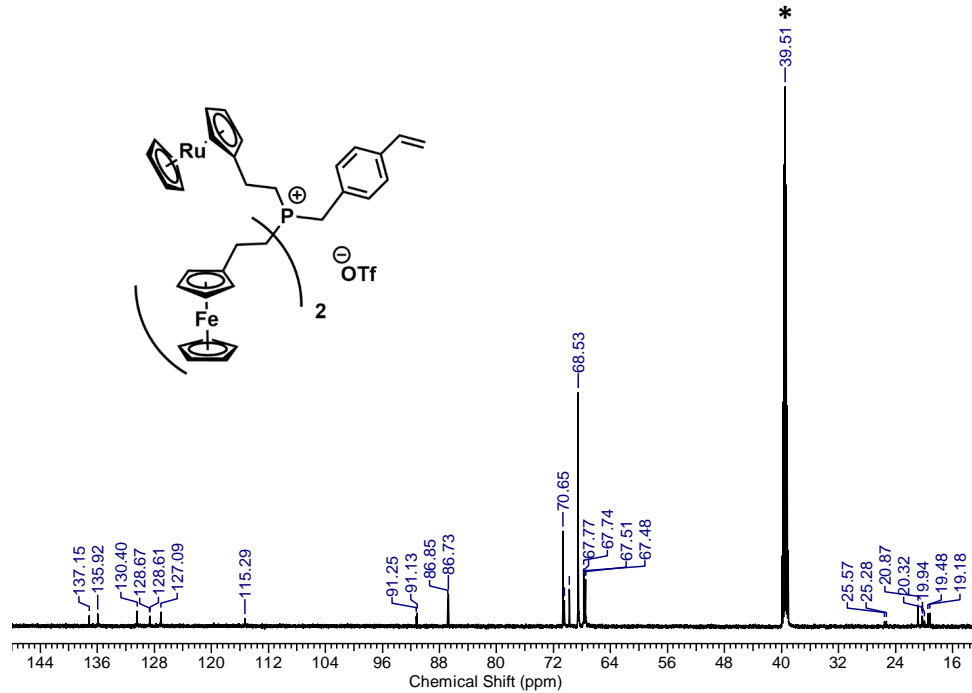


Fig. S12 $^{13}\text{C}\{^1\text{H}\}$ NMR spectrum of **7b** in $\text{DMSO}-d_6$. The asterisk denotes the solvent signal.

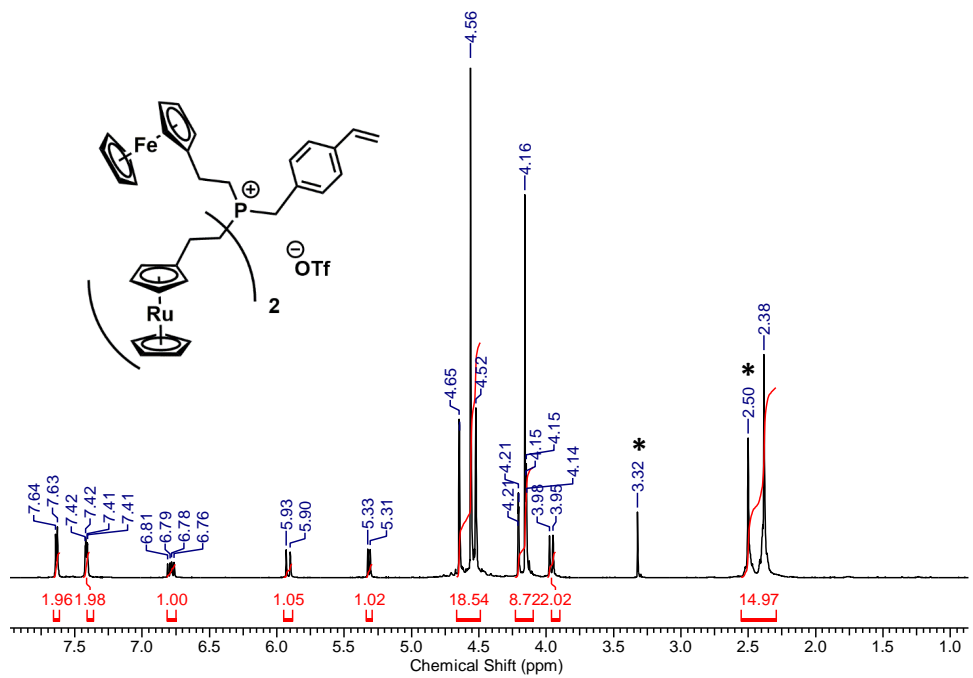


Fig. S13 ^1H NMR spectrum of **7c** in $\text{DMSO}-d_6$. The asterisks denote the solvent signals.

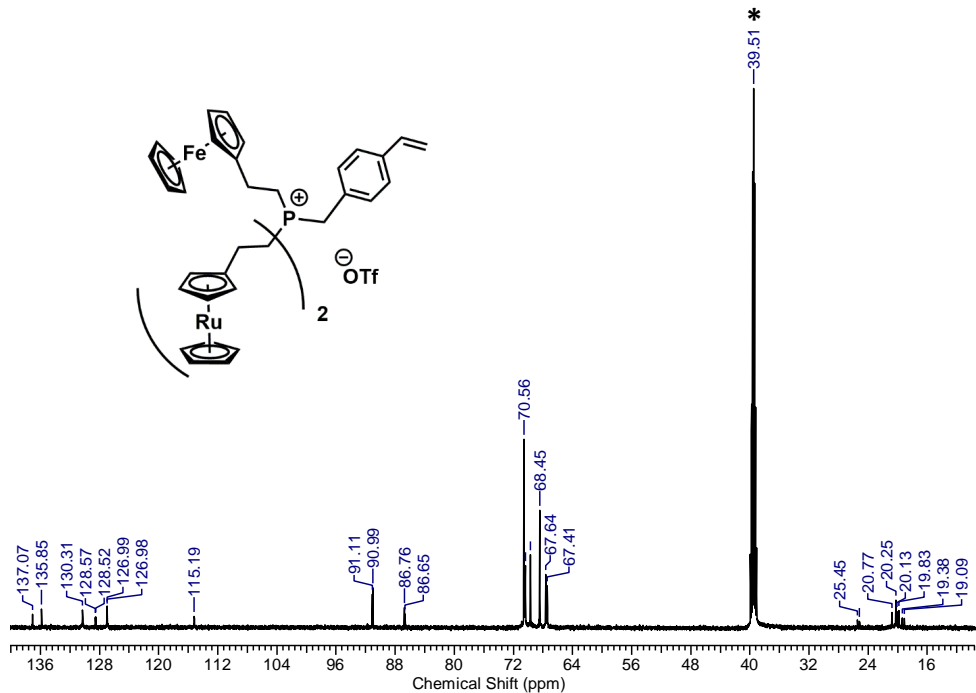


Fig. S14 $^{13}\text{C}\{^1\text{H}\}$ NMR spectrum of **7c** in $\text{DMSO}-d_6$. The quaternary carbon of the triflate anion was not detected. However, the purity of **7c** was confirmed by other methods such as ^{19}F NMR and elemental analysis. The asterisk denotes the solvent signal.

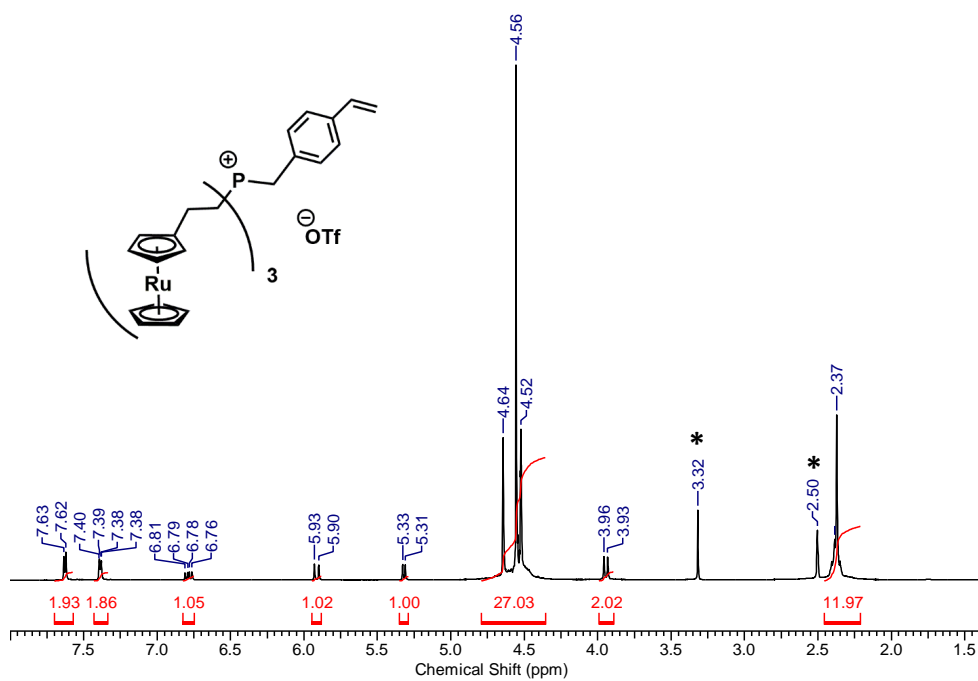


Fig. S15 ^1H NMR spectrum of **7d** in $\text{DMSO}-d_6$. The asterisks denote the solvent signals.

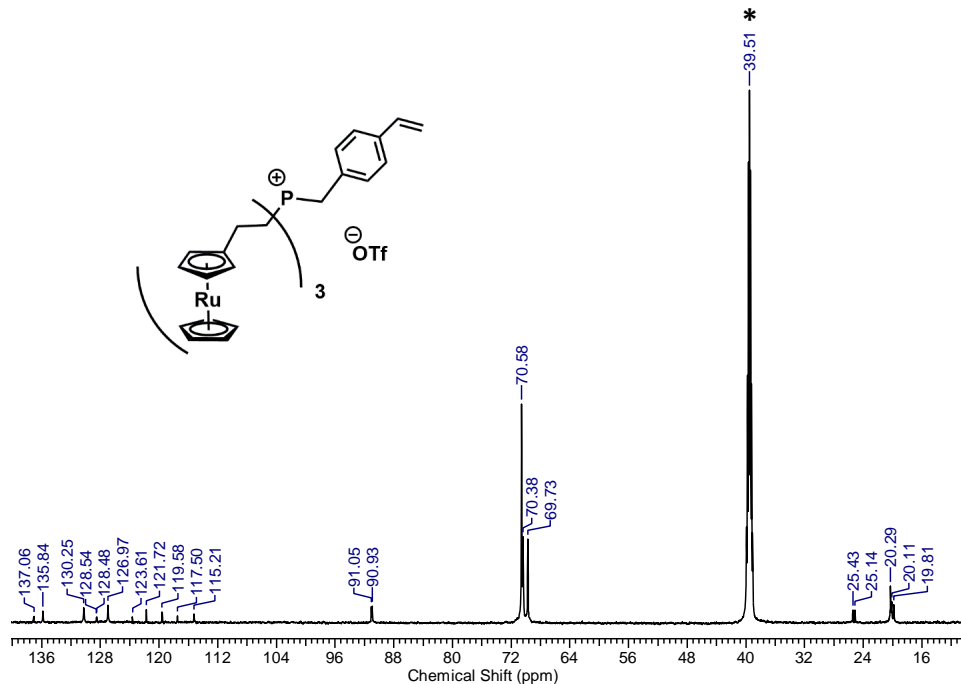


Fig. S16 $^{13}\text{C}\{^1\text{H}\}$ NMR spectrum of **7d** in $\text{DMSO}-d_6$. The asterisk denotes the solvent signal.

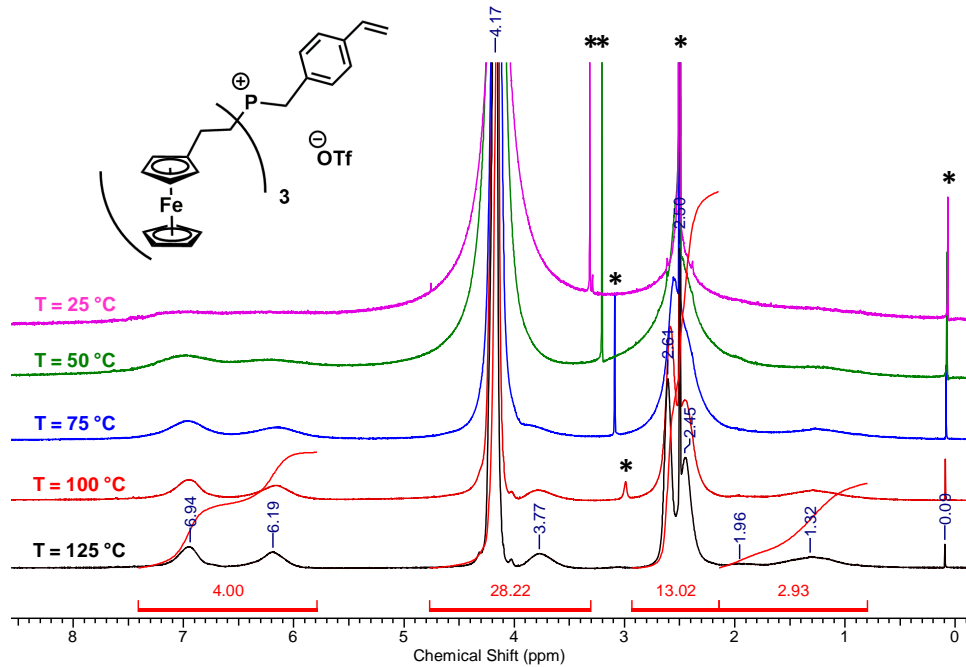


Fig. S17 ^1H NMR spectra of **8a** recorded at different temperatures in $\text{DMSO}-d_6$. The asterisks denote residual solvents signals and grease. Note – the residual water signal shifts upfield as temperature increases.

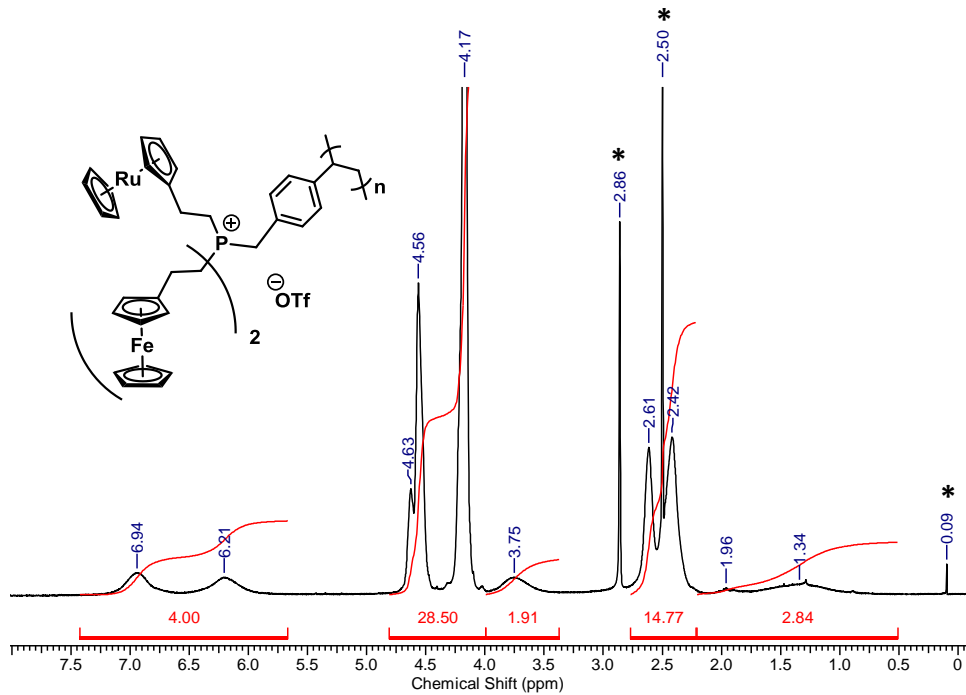


Fig. S18 ^1H NMR spectrum of **8b** recorded in $\text{DMSO}-d_6$ at $125\text{ }^{\circ}\text{C}$. The asterisks denote residual solvents signals and grease.

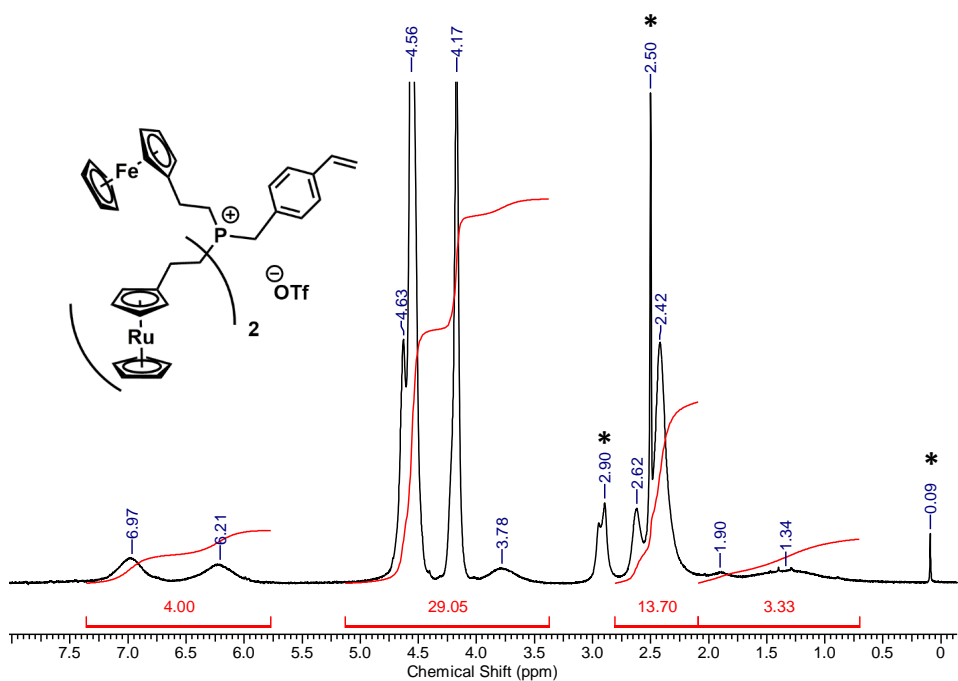


Fig. S19 ^1H NMR spectrum of **8c** recorded in $\text{DMSO}-d_6$ at $125\text{ }^\circ\text{C}$. The asterisks denote residual solvents signals and grease.

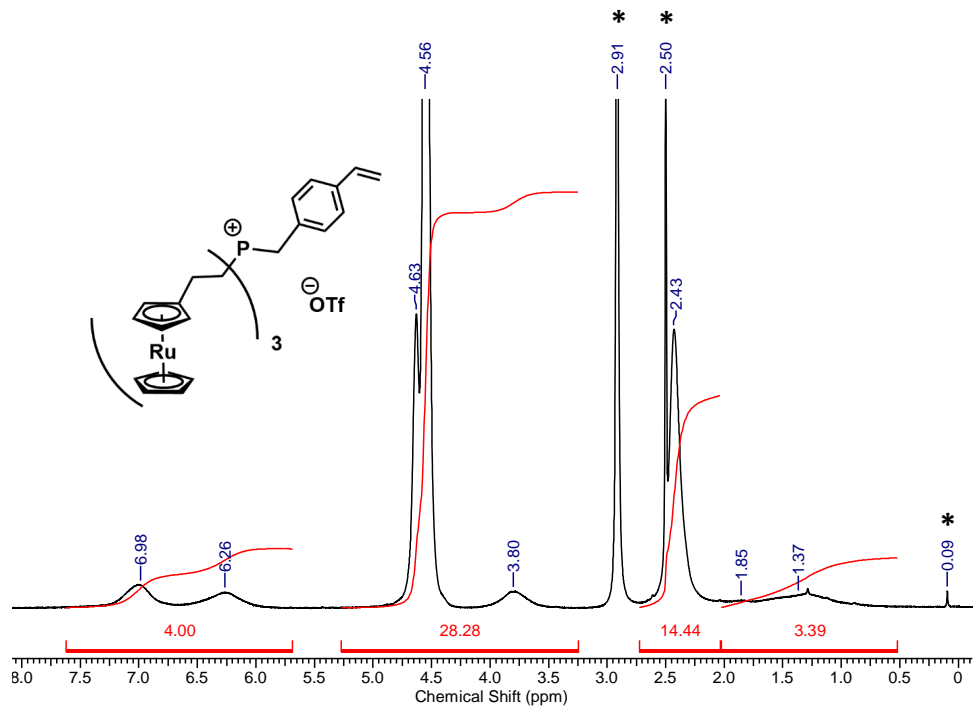


Fig. S20 ^1H NMR spectrum of **8d** recorded in $\text{DMSO}-d_6$ at $125\text{ }^\circ\text{C}$. The asterisks denote residual solvents signals and grease.

GPC data

Table S1 Conventional calibration GPC data for polyelectrolytes **8a–d**.

Sample	Injection	Max RI Response (mL)	M _n (Da)	M _w (Da)	M _w /M _n
8a	1	12.91	45,850	148,250	3.23
	2	12.91	46,300	147,100	3.18
	3	12.92	48,500	148,750	3.07
	Average	12.91	46,900	148,000	3.16
	Std. Dev.	0.00	1,162	699	0.069
	%RSD	0.04%	2.48%	0.47%	2.19%
8b	1	12.77	44,000	176,800	4.02
	2	12.77	46,150	183,550	3.98
	3	12.77	45,150	194,400	4.31
	Average	12.77	45,100	184,900	4.10
	Std. Dev.	0.00	887	7,262	0.147
	%RSD	0.02%	1.97%	3.93%	3.60%
8c	1	12.64	68,100	256,850	3.77
	2	12.61	69,350	284,700	4.10
	3	12.60	69,850	292,750	4.19
	Average	12.61	69,100	278,100	4.02
	Std. Dev.	0.02	751	15,389	0.18
	%RSD	0.12%	1.09%	5.53%	4.48%
8d	1	13.16	37,250	137,300	3.68
	2	13.15	40,100	146,000	3.64
	3	13.15	38,650	147,150	3.81
	Average	13.15	38,650	143,450	3.71
	Std. Dev.	0.00	1,150	4,398	0.07
	%RSD	0.04%	2.97%	3.07%	1.89%

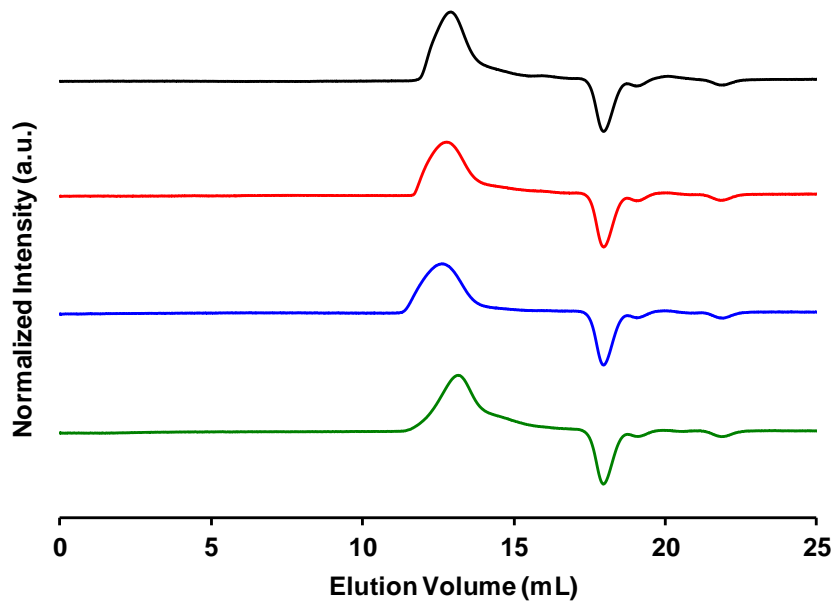


Fig. S21 GPC traces of polyelectrolytes **8a** ($3 \times$ Fc, black), **8b** ($2 \times$ Fc, $1 \times$ Rc; red), **8c** ($1 \times$ Fc, $2 \times$ Rc; blue), and **8d** ($3 \times$ Rc, green) recorded using a $60\text{ }^{\circ}\text{C}$ DMF solution containing 0.02 M [*n*-Bu₄N][OTf].

UV-vis absorption spectra

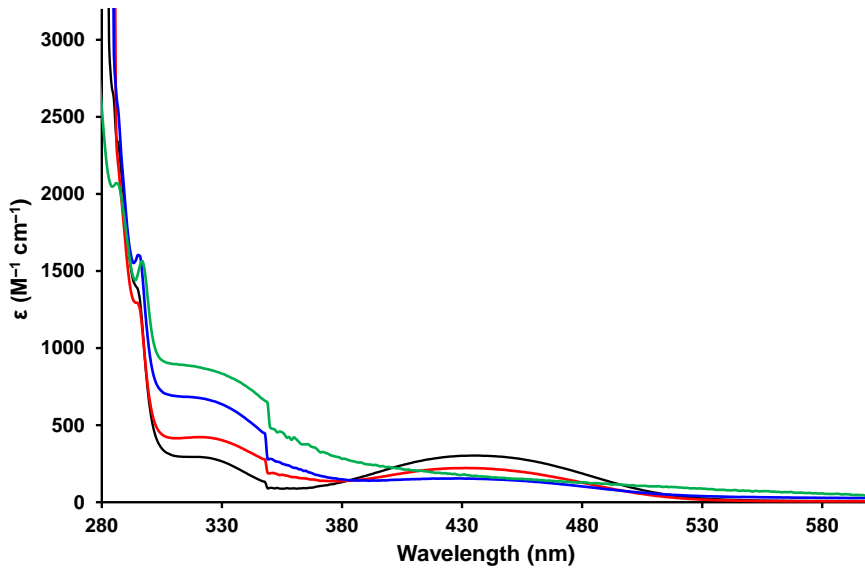


Fig. S22 UV-vis absorption spectra recorded for **6a** ($3 \times$ Fc; black), **6b** ($2 \times$ Fc, $1 \times$ Rc; red), **6c** ($1 \times$ Fc, $2 \times$ Rc; blue) and **6d** ($3 \times$ Rc; green) in THF.

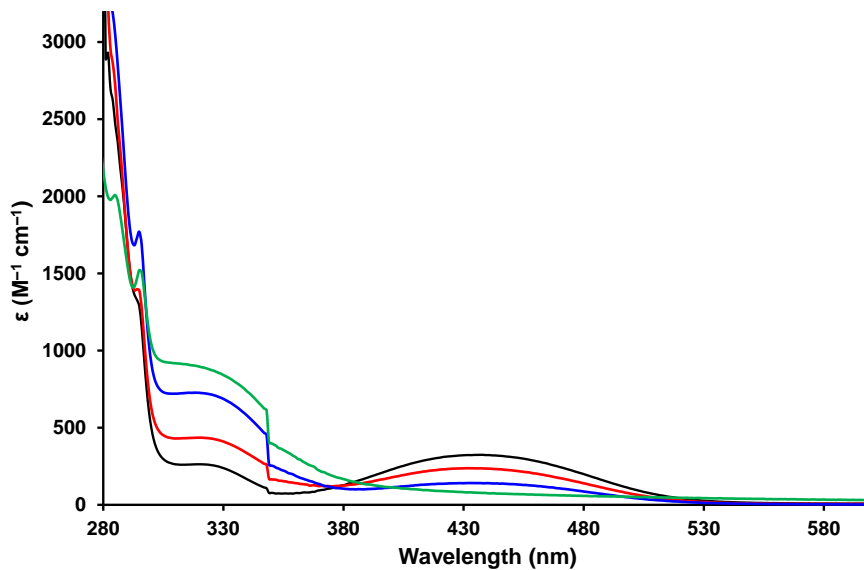


Fig. S23 UV-vis absorption spectra recorded for **7a** ($3 \times$ Fc; black), **7b** ($2 \times$ Fc, $1 \times$ Rc; red), **7c** ($1 \times$ Fc, $2 \times$ Rc; blue) and **7d** ($3 \times$ Rc; green) in THF.

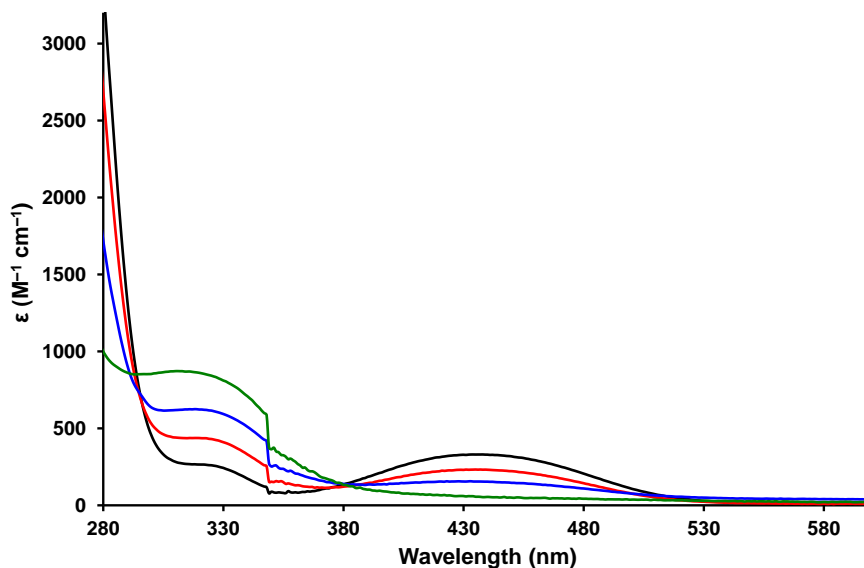


Fig. S24 UV-vis absorption spectra recorded for **8a** ($3 \times$ Fc; black), **8b** ($2 \times$ Fc, $1 \times$ Rc; red), **8c** ($1 \times$ Fc, $2 \times$ Rc; blue) and **8d** ($3 \times$ Rc; green) in THF.

Cyclic voltammograms

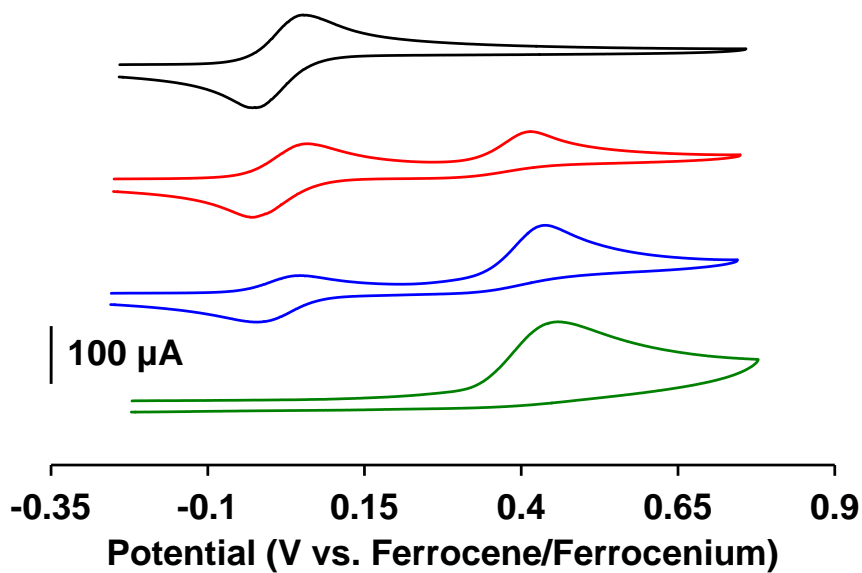


Fig. S25 Cyclic voltammograms of monomers **7a** ($3 \times \text{Fc}$; black), **7b** ($2 \times \text{Fc}, 1 \times \text{Rc}$; red), **7c** ($1 \times \text{Fc}, 2 \times \text{Rc}$; blue), and **7d** ($3 \times \text{Rc}$; green) recorded at 250 mV s^{-1} in solutions of 2/1 $\text{CH}_2\text{Cl}_2/\text{MeCN}$ containing $0.1 \text{ M } [n\text{-Bu}_4\text{N}][\text{OTf}]$ as supporting electrolyte.

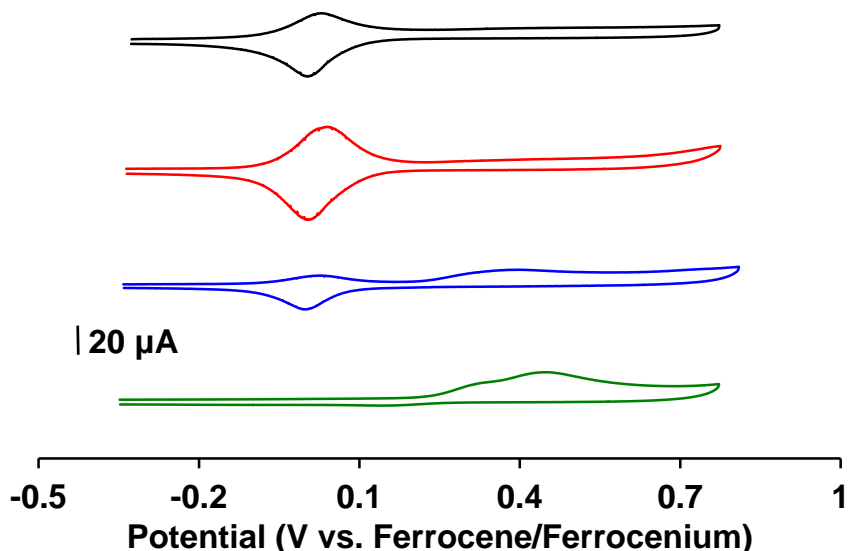


Fig. S26 Cyclic voltammograms of polyelectrolytes: **8a** ($3 \times \text{Fc}$, black), **8b** ($2 \times \text{Fc}, 1 \times \text{Rc}$; red), **8c** ($1 \times \text{Fc}, 2 \times \text{Rc}$; blue), and **8d** ($3 \times \text{Rc}$, green) recorded at 250 mV s^{-1} in solutions of 2/1 $\text{CH}_2\text{Cl}_2/\text{MeCN}$ containing $0.1 \text{ M } [n\text{-Bu}_4\text{N}][\text{OTf}]$ as supporting electrolyte. Note – due to the limited and different solubilities of the polyelectrolytes in the solvent/electrolyte mixture, the intensities of the waves in the recorded cyclic voltamograms were lower compared to that of the corresponding monomers and also a clear trend was not observed when their cyclic voltamograms were compared. Furthermore, due to low concentration and extreme broadening, the irreversible oxidation wave of ruthenocene for **8b** was not observed.

Differential scanning calorimetry thermograms

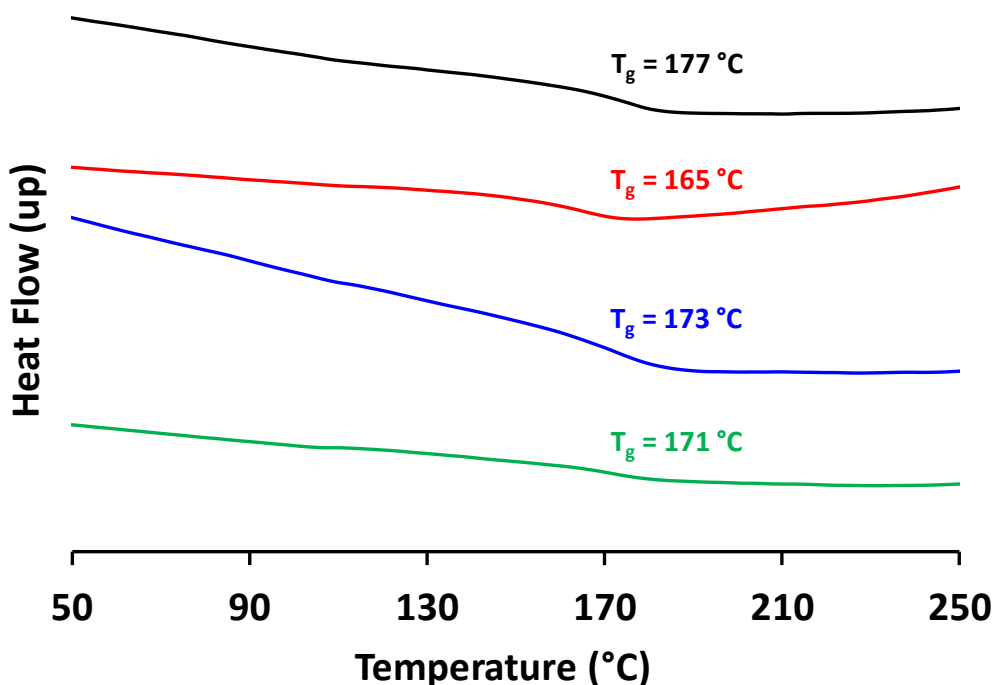


Fig. S27 DSC thermograms of polyelectrolytes **8a** ($3 \times F_c$, black), **8b** ($2 \times F_c, 1 \times R_c$; red), **8c** ($1 \times F_c, 2 \times R_c$; blue), and **8d** ($3 \times R_c$, green) recorded at a scan rate of 10 °C min^{-1} .

Scanning electron microscopy and energy-dispersive X-ray spectroscopy results

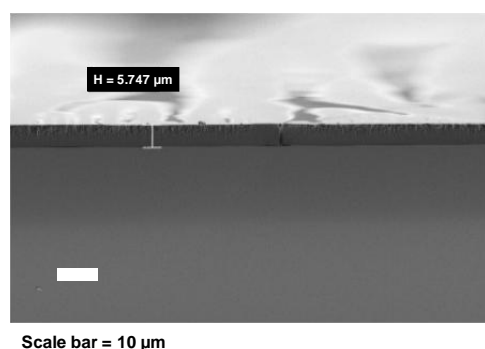


Fig. S28 SEM of a cross section of a representative drop-cast film of polyelectrolyte **8a**.

Element maps

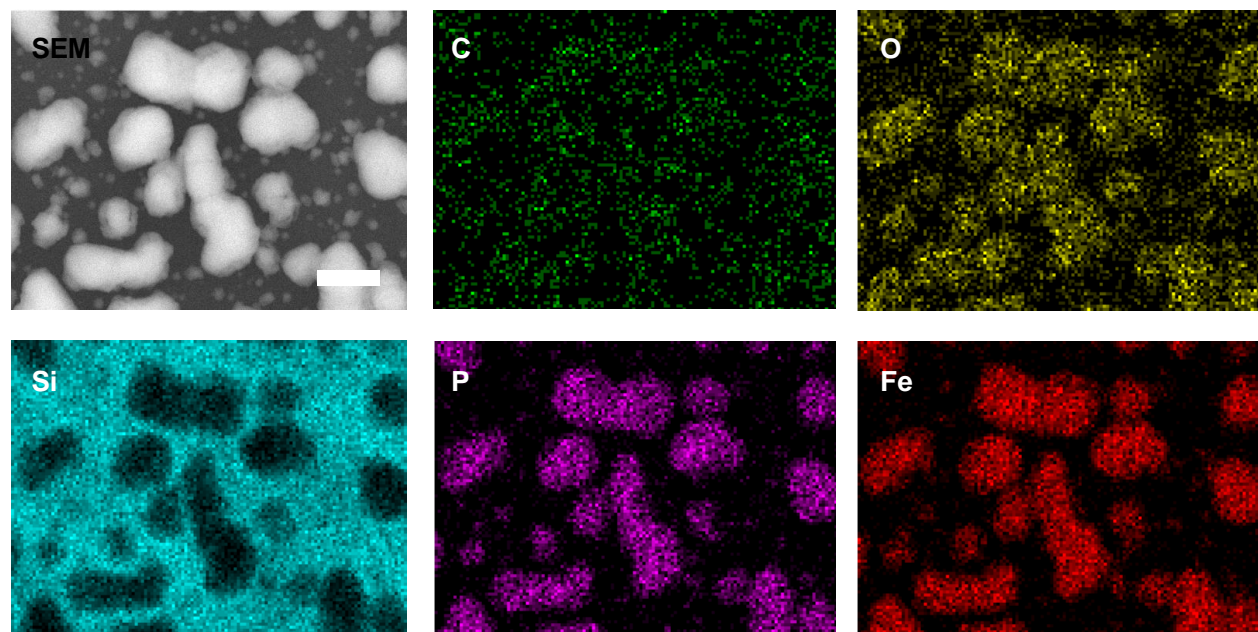


Fig. S29 SEM image and elemental maps (C, O, Si, P, Fe) for the nanomaterials prepared via the pyrolysis of a film of polyelectrolyte **8a**. Scale bar = 1 μm .

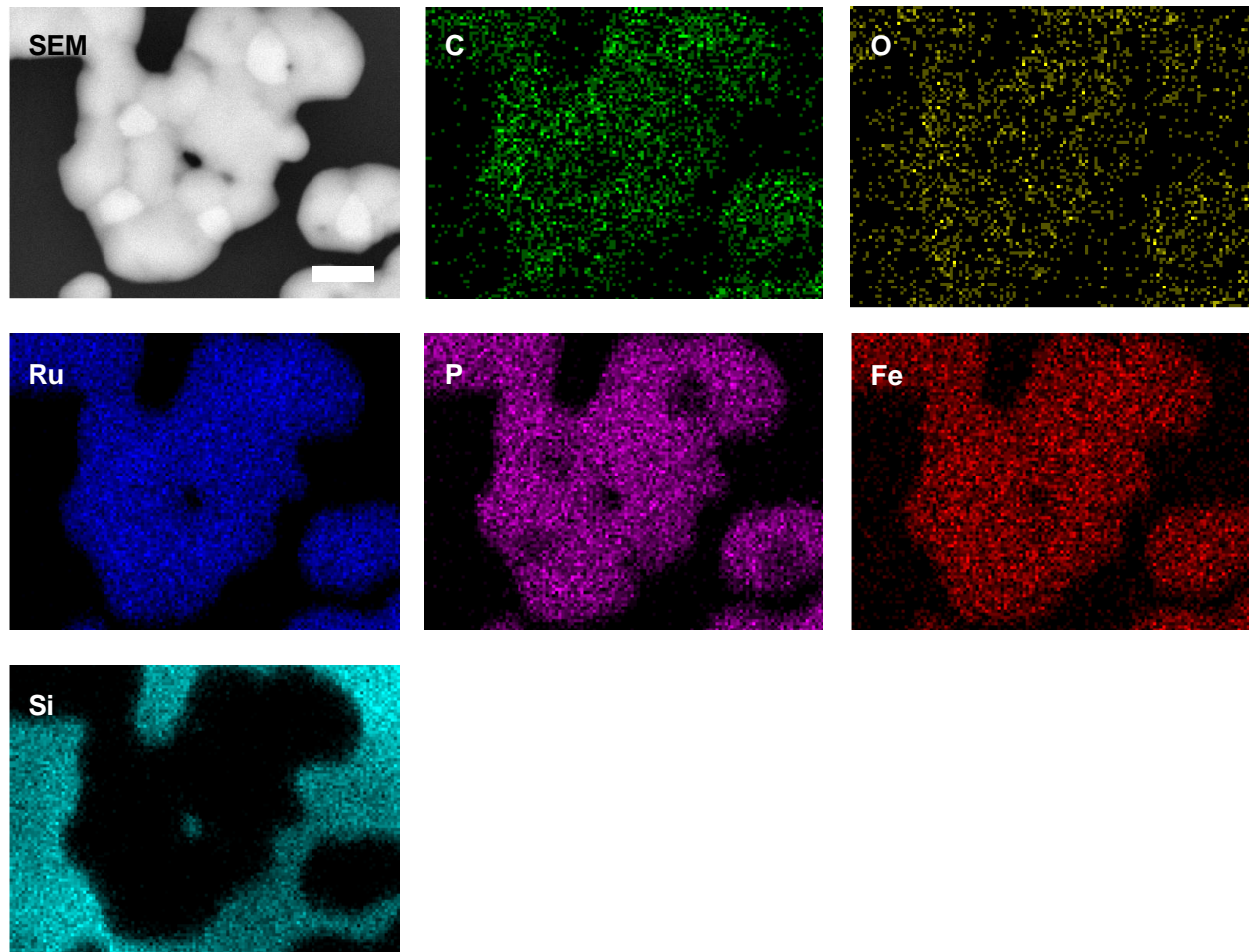


Fig. S30 SEM image and elemental maps (C, O, Ru, P, Fe, Si) for the nanomaterials prepared via the pyrolysis of a film of polyelectrolyte **8c**. Scale bar = 1 μm .

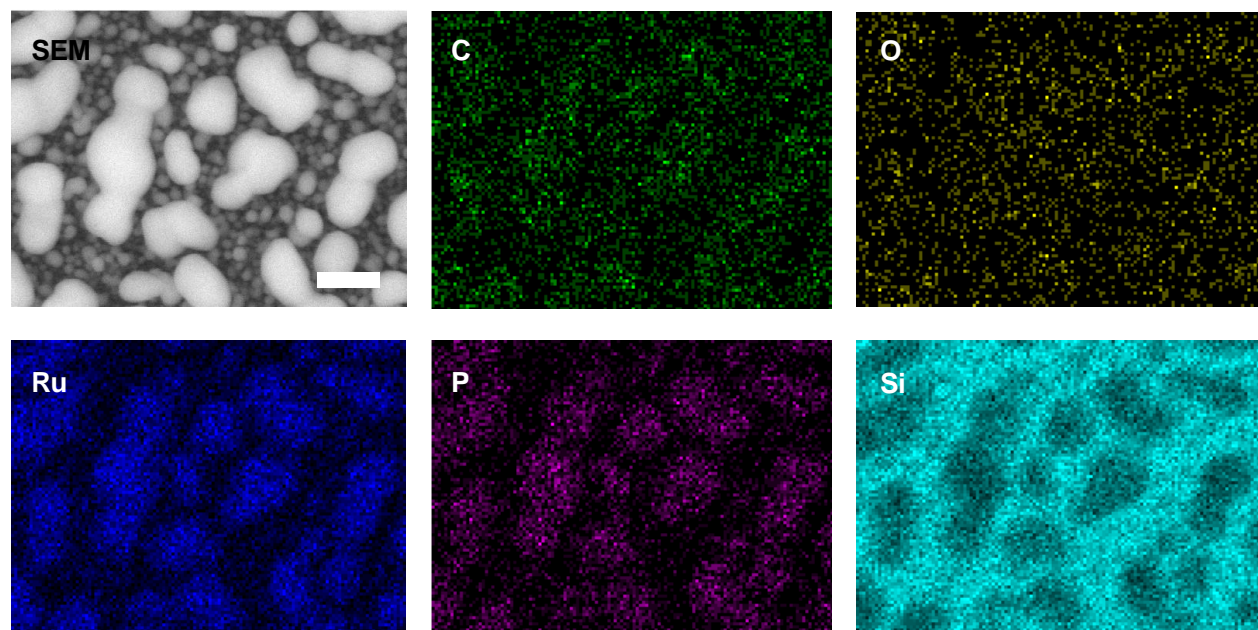
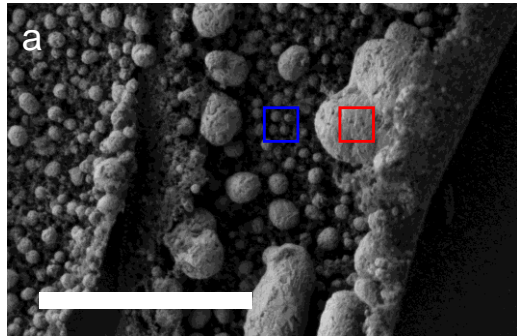


Fig. S31 SEM image and elemental maps (C, O, Ru, P, Si) for the nanomaterials prepared via the pyrolysis of a film of polyelectrolyte **8d**. Scale bar = 350 nm.

Scanning electron microscopy and energy-dispersive X-ray spectroscopy results

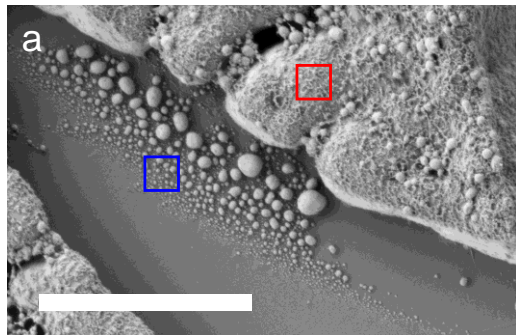


b

	% ^a	C	O	P	Fe
<i>Bulk</i>	20.6	18.6	21.3	39.4	
	25.1	25.4	17.1	32.5	
	25.3	28.8	16.3	29.5	
	23.9	21.3	19.8	34.9	
	20.2	29.2	14.3	36.4	
Average	23.0 ± 2.5	24.7 ± 4.6	17.7 ± 2.8	34.6 ± 3.8	
<i>Particles</i>	36.9	27.1	11.1	24.9	
	33.7	25.8	10.4	30.1	
	46.3	26.9	8.2	18.6	
	78.1	20.0	0.5	1.4	
	79.5	18.6	0.7	1.3	
	80.4	17.9	0.5	1.1	
	48.6	33.0	7.5	10.9	
	52.4	30.0	7.3	10.3	
Average	57.0 ± 19.5	24.9 ± 5.5	5.8 ± 4.5	12.3 ± 11.2	

^aData normalized to exclude silicon detected from substrate.

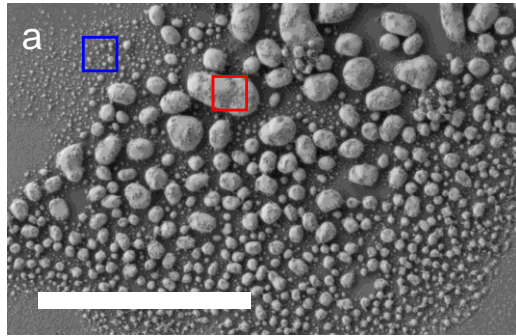
Fig. S32 (a) Representative SEM image illustrating the areas analyzed to determine the elemental composition of dense regions of relatively large particles (*bulk*) and less dense regions of relatively small particles (*particles*) produced via the pyrolysis of a film of polyelectrolyte **8a**. (b) Data table summarizing the elemental composition of multiple areas of the silicon wafer determined using EDX spectroscopy. Scale bar = 5 μm .



b	% ^a	C	O	P	Fe	Ru
<i>Bulk</i>	14.1	25.9	16.3	26.8	16.9	
	3.8	20.9	10.7	38.4	26.2	
	10.9	44.7	11.8	23.6	8.9	
	14.0	24.4	16.0	28.6	17.0	
	13.2	27.3	16.2	26.1	17.1	
	13.9	26.2	18.8	21.9	19.3	
	16.6	25.4	18.8	20.5	18.7	
	14.9	28.5	18.5	19.6	18.5	
	13.2	27.4	19.4	20.5	19.4	
	13.9	25.6	16.0	27.6	16.9	
	12.3	26.6	15.9	28.5	16.8	
Average		12.8 ± 3.3	27.5 ± 6.0	16.2 ± 2.8	25.6 ± 5.4	17.8 ± 4.0
<i>Particles</i>	16.2	30.7	14.9	24.0	14.2	
	38.6	36.6	8.6	8.3	8.0	
	26.7	34.2	12.1	16.5	10.4	
	15.5	42.4	12.1	22.1	7.8	
	21.2	28.6	14.3	22.3	13.7	
Average		23.6 ± 9.5	34.5 ± 5.4	12.4 ± 2.5	18.7 ± 6.4	10.8 ± 3.0

^aData normalized to exclude silicon detected from substrate.

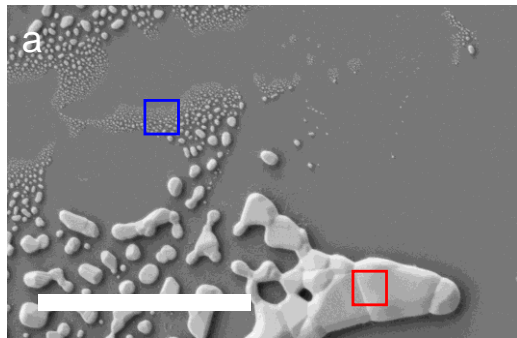
Fig. S33 (a) Representative SEM image illustrating the areas analyzed to determine the elemental composition of dense regions of relatively large particles (*bulk*) and less dense regions of relatively small particles (*particles*) produced via the pyrolysis of a film of polyelectrolyte **8b**. (b) Data table summarizing the elemental composition of multiple areas of the silicon wafer determined using EDX spectroscopy. Scale bar = 5 μm.



b	% ^a	C	O	P	Fe	Ru
<i>Bulk</i>	14.5	44.2	12.9	6.7	21.6	
	14.6	46.5	12.0	6.6	20.2	
	13.2	42.9	13.6	7.4	22.9	
	13.7	42.0	13.7	7.3	23.3	
	28.9	16.3	18.4	8.0	28.5	
	22.1	14.9	20.3	9.6	33.2	
	31.9	20.0	16.0	6.9	25.2	
	Average	19.8 ± 7.8	32.4 ± 14.5	15.3 ± 3.1	7.5 ± 1.0	25.0 ± 4.5
<i>Particles</i>	16.0	48.9	9.4	6.6	19.1	
	13.5	54.2	6.9	7.9	17.5	
	70.6	19.5	2.8	1.6	5.4	
	74.2	15.4	3.1	1.6	5.7	
	64.7	26.1	2.6	1.5	5.0	
	63.1	10.9	10.4	3.1	12.5	
	62.8	11.6	9.8	3.3	12.6	
	Average	52.1 ± 25.9	26.6 ± 17.8	6.4 ± 3.5	3.7 ± 2.6	11.1 ± 5.9

^aData normalized to exclude silicon detected from substrate.

Fig. S34 (a) Representative SEM image illustrating the areas analyzed to determine the elemental composition of dense regions of relatively large particles (*bulk*) and less dense regions of relatively small particles (*particles*) produced via the pyrolysis of a film of polyelectrolyte **8c**. (b) Data table summarizing the elemental composition of multiple areas of the silicon wafer determined using EDX spectroscopy. Scale bar = 5 μm.



b

% ^a	C	O	P	Ru
<i>Bulk</i>	16.1	5.2	25.5	53.1
	17.8	5.2	25.1	51.9
	17.6	5.1	25.0	52.3
	18.3	5.0	25.0	51.7
	20.9	6.1	23.9	49.1
Average	18.1 ± 1.8	5.3 ± 0.4	24.9 ± 0.6	51.6 ± 1.5
<i>Particles</i>	71.4	20.6	3.2	4.8
	76.0	16.4	3.1	4.6
	69.7	18.9	4.6	6.8
	72.1	15.4	5.1	7.4
	74.2	19.6	2.3	4.0
Average	72.7 ± 2.4	18.2 ± 2.2	3.6 ± 1.2	5.5 ± 1.5

^aData normalized to exclude silicon detected from substrate.

Fig. S35 (a) Representative SEM image illustrating the areas analyzed to determine the elemental composition of dense regions of relatively large particles (*bulk*) and less dense regions of relatively small particles (*particles*) produced via the pyrolysis of a film of polyelectrolyte **8d**. (b) Data table summarizing the elemental composition of multiple areas of the silicon wafer determined using EDX spectroscopy. Scale bar = 5 μm.

Powder X-ray diffractograms

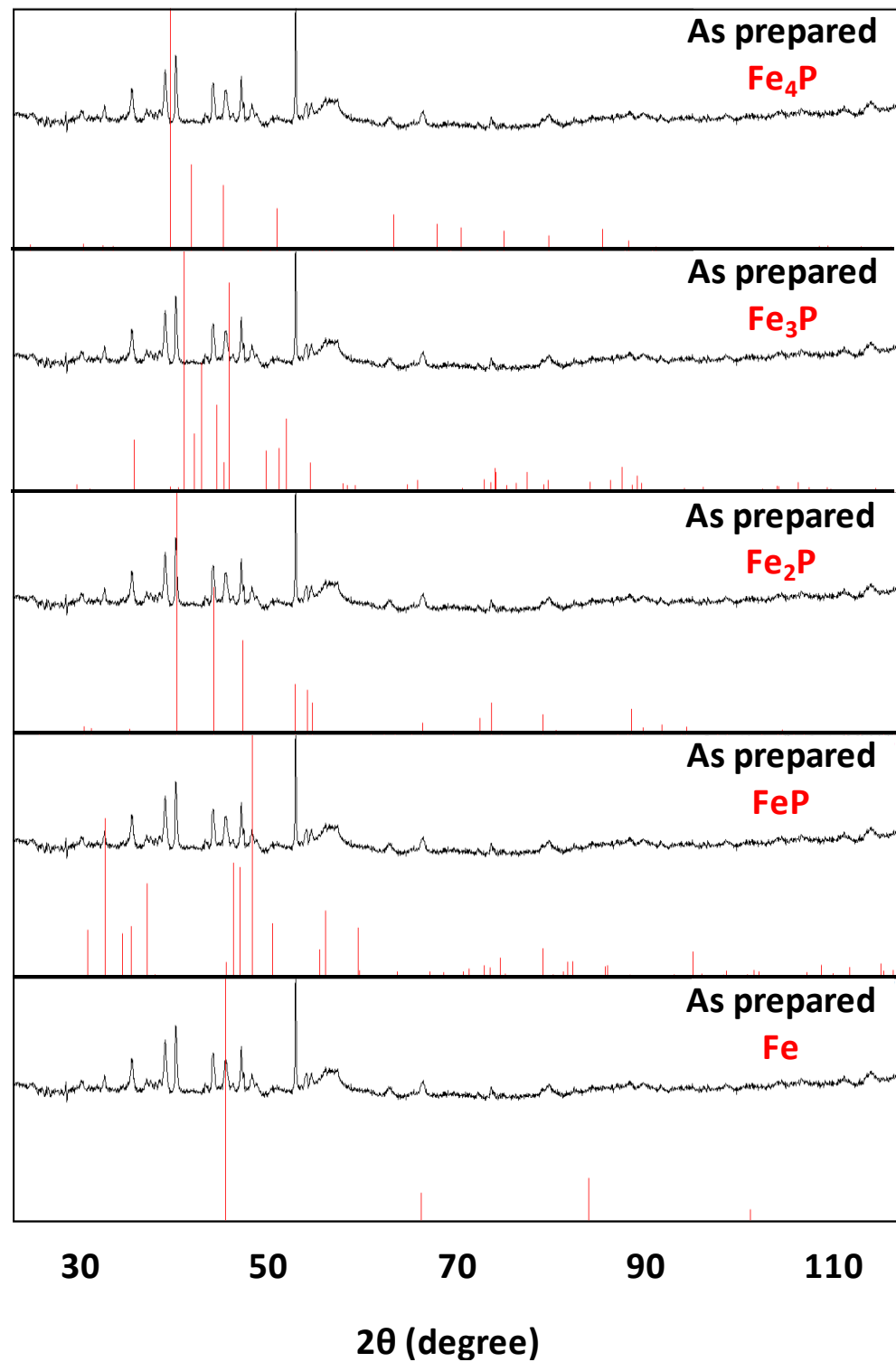


Fig. S36 Powder X-ray diffractogram of the nanomaterials prepared via pyrolysis of a film of **8a** plotted vs. iron phosphides and iron.¹

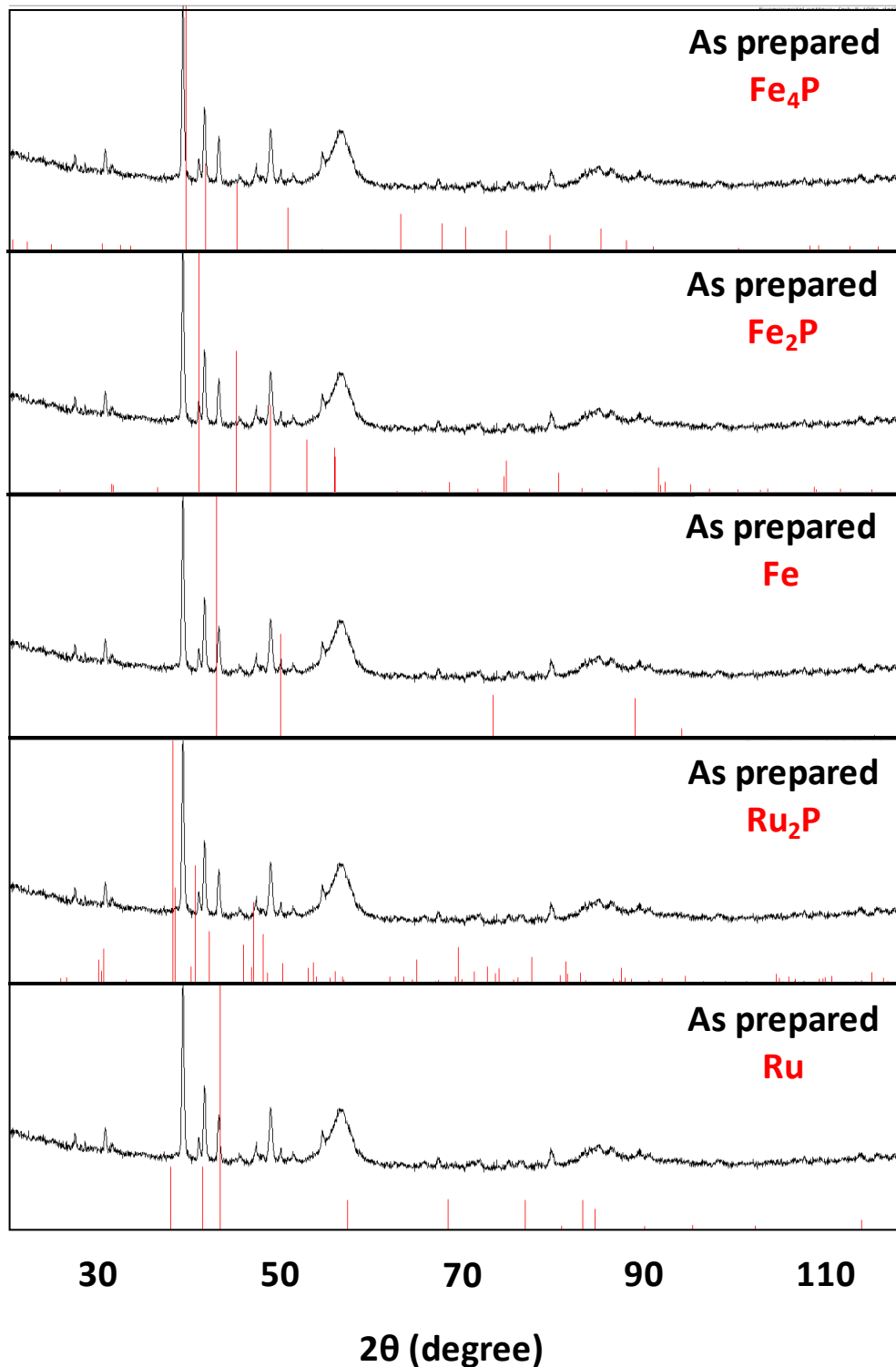


Fig. S37 Powder X-ray diffractogram of the nanomaterials prepared via pyrolysis of a film of **8b** plotted vs. iron phosphides, iron, ruthenium phosphides and ruthenium.¹

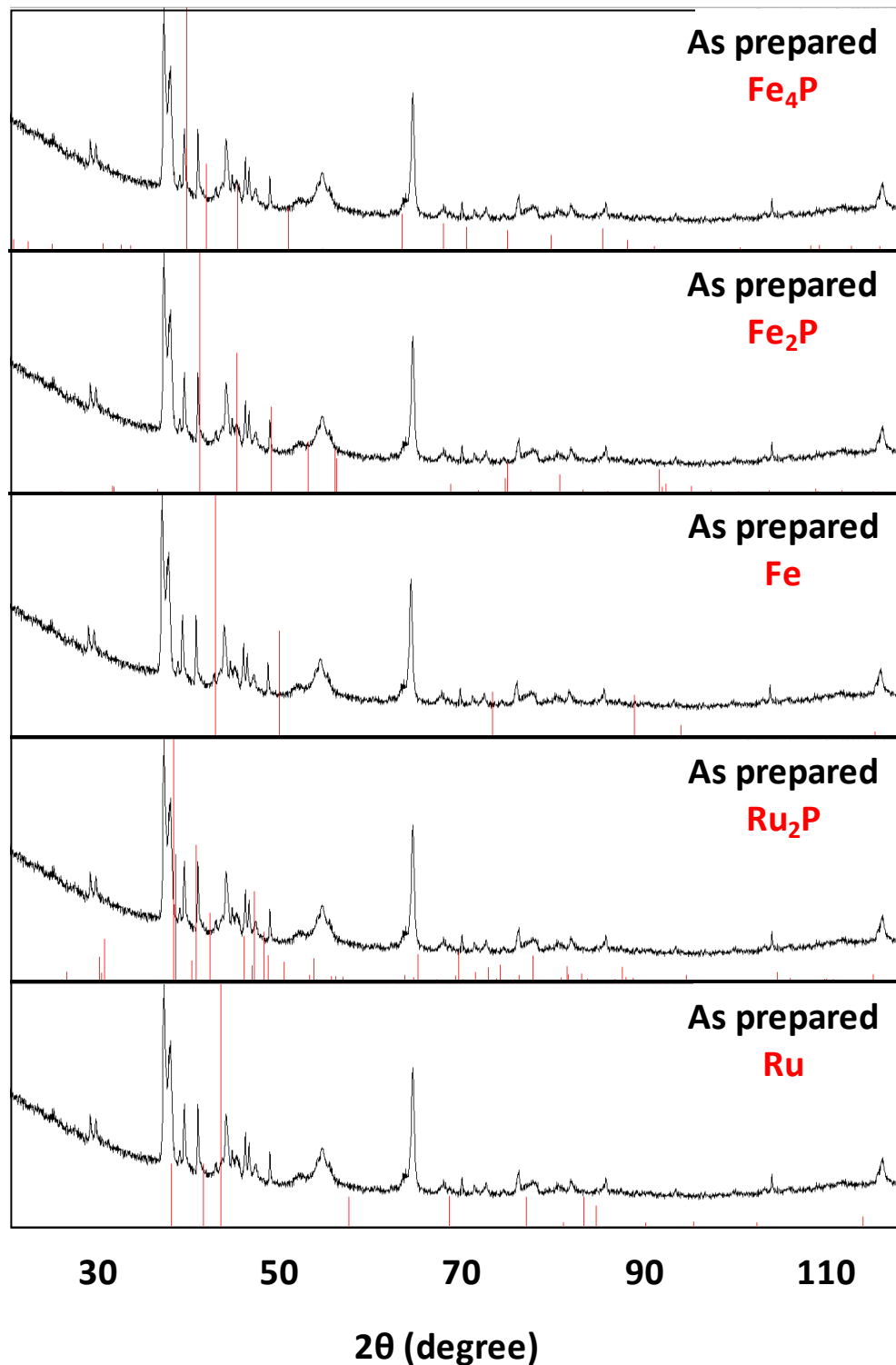


Fig. S38 Powder X-ray diffractogram of the nanomaterials prepared via pyrolysis of a film of **8c** plotted vs. iron phosphides, iron, ruthenium phosphides and ruthenium.¹

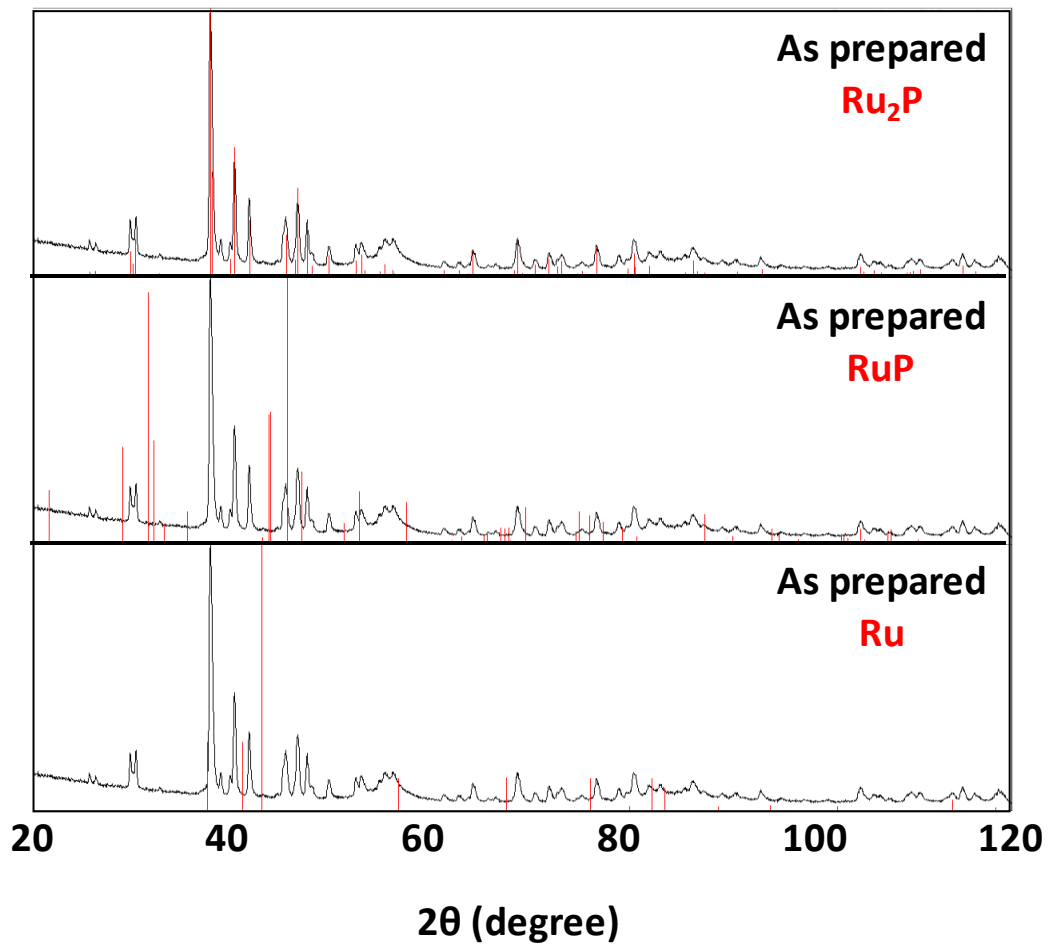


Fig. S39 Powder X-ray diffractogram of the nanomaterials prepared via pyrolysis of a film of **8d** plotted vs. ruthenium phosphides and ruthenium.¹

References

- 1 The PXRD patterns were compared using the ICSD database and PDF4+ software.